*Cardiovascular Engineering and Technology*, Vol. 13, No. 2, April 2022 *(© 2021)* pp. 331–342
https://doi.org/10.1007/s13239-021-00580-5

*Original Article*

# A 1D–3D Hybrid Model of Patient-Specific Coronary Hemodynamics

Noelia Grande Gutiérrez,[1] Talid Sinno,[1] and Scott L. Diamond [1,2]

[1]Department of Chemical and Biomolecular Engineering, University of Pennsylvania, Philadelphia, USA; and [2]Department of Bioengineering, University of Pennsylvania, Philadelphia, USA

*(Received 14 May 2021; accepted 7 September 2021; published online 30 September 2021)*

Associate Editor Igor Efimov oversaw the review of this article.

**Abstract**
*Purpose*—Coronary flow is affected by evolving events such as atherosclerotic plaque formation, rupture, and thrombosis, resulting in myocardial ischemia and infarction. Highly resolved 3D hemodynamic data at the stenosis is essential to model shear-sensitive thrombotic events in coronary artery disease.
*Methods*—We developed a hybrid 1D–3D simulation framework to compute patient-specific coronary hemodynamics efficiently. A 1D model of the coronary flow is coupled to an image-based 3D model of the region of interest. This framework affords the advantages of reduced-order modeling, decreasing the global computational cost, without sacrificing the accuracy of the quantities of interest.
*Results*—We validated our 1D–3D model against full 3D coronary simulations in healthy and diseased conditions. Our results showed good agreement between the 3D and the 1D–3D models while reducing the computational cost by 40-fold compared to the 3D simulation. The 1D–3D model predicted left/right coronary flow distribution within 3% and provided an accurate estimation of fractional flow reserve and wall shear stress distribution at the stenosis comparable to the 3D simulation.
*Conclusion*—Savings in computational cost may be significant in situations with changing geometry, such as growing thrombosis. Also, this approach would allow quantifying the time-dependent effect of thrombotic growth and occlusion on the global coronary circulation.

**Keywords—**Hemodynamics, Coronary artery disease, Coronary stenosis, Image-based modeling, Reduced-order modeling.

## INTRODUCTION

Thrombosis is a dangerous complication associated with cardiovascular disease, resulting in myocardial infarction and stroke, both leading causes of death globally. In patients with coronary artery disease (CAD), local stenosis creates extreme hemodynamic and mechanobiological conditions that can trigger occlusive thrombosis.[5,25] In particular, low and oscillatory shear stress localizes endothelial dysfunction and atherosclerosis.[20] As plaque reduces the vessel lumen diameter, local hemodynamics can influence plaque rupture, platelet aggregation and thrombus growth.[23,25,28,29] Therefore, patient-specific coronary hemodynamics should be considered in a comprehensive model of coronary thrombotic occlusion.

Three-dimensional (3D) image-based modeling and computational fluid dynamics are well-validated for simulating coronary blood flow. However, 3D flow simulations of the whole coronary tree involve a high computational cost. Therefore, they could become a bottleneck considering cases with a significantly wide range of scales or time-evolving problems, such as thrombosis. Reduced-order models—on their own or coupled with higher-dimensional models—provide a computationally feasible alternative to full 3D patient-specific blood flow modeling.[6,10,13,15,30,36,39] Recent studies have demonstrated the potential of one-dimensional (1D) models to obtain coronary hemodynamic data, including the estimation of fractional flow reserve (FFR), the gold standard for evaluating the functional significance of the stenosis in CAD patients.[1,7,14,21,43] However, 1D models do not provide a spatially resolved description of the local flow conditions, i.e., the mechanical and biochemical environment, in the vicinity of the stenotic lesion where the thrombus may eventually form. This is problematic

Address correspondence to Scott L. Diamond, Department of Chemical and Biomolecular Engineering, University of Pennsylvania, Philadelphia, USA. Electronic mail: sld@seas.upenn.edu

because a detailed characterization of the local hemodynamic conditions is necessary to appropriately model thrombus formation following plaque rupture or erosion. On the other hand, 3D submodels focused on the stenotic region alone do not incorporate time-dependent patient-specific hemodynamic information. For example, thrombosis models in 2D and 3D have been based on idealized geometries and flow conditions.[9,18,19,40–42,45] and consider relatively small computational domains (~ 10–100 $\mu$m) localized in the proximity of a tissue factor (TF) source.

A coupled 1D–3D approach can address the limitations described above by offering significantly reduced computational cost while preserving the accuracy of the local hemodynamics in the region of interest, that is, the stenosis. A 1D–3D coupled model of the coronary blood flow provides patient-specific boundary conditions for a localized stenosis model and at the same time allows the quantification of the effect of the occlusion, as it progresses, on the global coronary circulation. Coupled 1D–3D models have been introduced previously to evaluate the effect of global flow conditions on local hemodynamics and vice versa.[3,12,24] In particular, prior studies have proposed a hybrid 1D–3D approach in settings such as cerebral aneurysms, abdominal/femoral aorta and carotid arteries by Urquiza *et al.* and Blanco *et al.*[2–4,35] Here, we present the first 1D–3D coupled model of the coronary circulation. The proposed framework computes dynamic (i.e., pulsatile), patient-specific and highly resolved hemodynamic conditions at a lower computational cost, providing a computationally feasible alternative for modeling coronary hemodynamics. The main goal of this paper is to verify the accuracy of our hybrid 1D–3D coronary model compared to a full 3D simulation and demonstrate its potential to be used for multi-scale patient-specific coronary simulations.

## MATERIALS AND METHODS

### *Three-Dimensional Computational Fluid Dynamics (3D CFD)*

A 3D anatomical model of the coronary tree can be generated using non-invasive image data, in particular Computed Tomography Angiography (CTA), *via* image segmentation. In this case, we constructed a baseline coronary tree anatomy based on a healthy subject CTA in *SimVascular*, an open-source package for cardiovascular modeling.[34] To construct this model we used the normal coronary case available in www.simvascular.com as a reference. We used this coronary tree as the healthy reference for our computational experiments. Then, we virtually introduced a stenosis with a 90% area reduction in the left anterior descending (LAD) artery to test the proposed modeling framework in a diseased case. The minimum area location was positioned at 2 cm from the bifurcation, between two healthy segmentations of the native vessel set 1 cm apart. The longitudinal variation of the radius is obtained *via* interpolation between the prescribed 2D segmentations directly in *Simvascular*. A finite element 3D mesh was generated using Tetgen,[31] including a boundary layer mesh and mesh refinement at the stenosis. The boundary layer consists of three layers with a 70% layer-decreasing ratio. Local refinement was defined from the proximal section of the stenosis to a distal point at least ten diameters downstream.[44] Maximum edge size for coronary mesh and the local mesh refinement was set to 0.06 cm and 0.025 cm respectively based on mesh independence analysis. Blood flow was modeled using the Navier–Stokes equations

$$\nabla \cdot \boldsymbol{u} = 0 \tag{1}$$

$$\rho \boldsymbol{u}_t + \rho(\mathbf{u} \cdot \nabla)\mathbf{u} = -\nabla p + \nabla \bar{\bar{\tau}} \tag{2}$$

$$\bar{\bar{\tau}} = \mu\left(\nabla \boldsymbol{u} + \nabla \boldsymbol{u}^{\boldsymbol{T}}\right) \tag{3}$$

These equations were solved using the fluid 3D solver available in *SimVascular* to obtain fully spatially and temporally resolved velocity $\boldsymbol{u}(X,t)$ and pressure fields $p(X,t)$. In this case, we considered a rigid wall approximation to model the arterial wall. Blood was modeled as an incompressible Newtonian fluid with density = 1060 kg m$^{-3}$ and dynamic viscosity = 0.004 kg m$^{-1}$ s$^{-1}$.

### *One-Dimensional (1D) Hemodynamic Model*

From the 3D anatomical model, we extracted the centerlines and corresponding luminal diameters for the different segments of the coronary tree to obtain a 1D representation of the model. Each coronary segment was assigned a length and initial and final cross-sectional areas, and was discretized into 1D finite elements. Element size for the 1D model was set to 0.1 cm. A canonical representation of the coronary tree including the main coronary artery segments is presented in Fig. 1. A summary of the geometrical definition of this model is presented in Table S1 included in the Electronic Supplementary Material (ESM) Section 1.

The 1D flow equations can be obtained by integrating the 3D Navier–Stokes equations over the vessel cross-section[13,15] assuming that the velocity varies primarily along the vessel centerline. The resulting

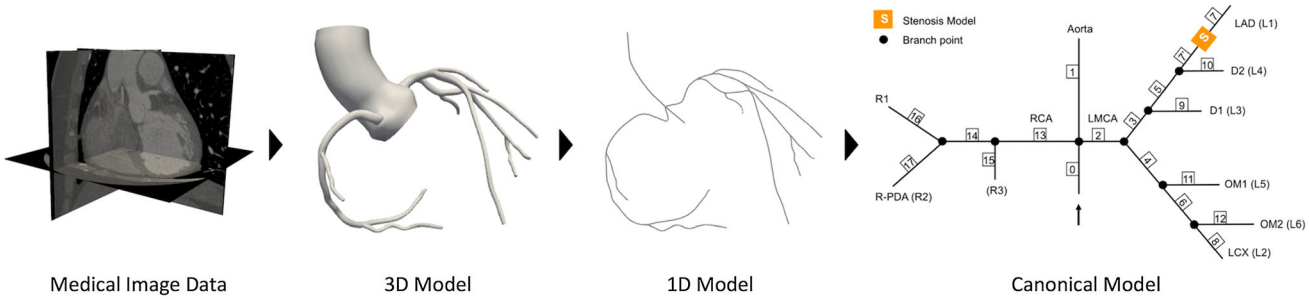


**FIGURE 1. Modeling pipeline. From image data (CTA) to canonical 1D representation of the coronary tree. Reference for a healthy coronary tree.**

conservation of mass and momentum equations can be written as follows:

$$\frac{\partial A}{\partial t}+\frac{\partial Q}{\partial x}=0, \tag{4}$$

$$\frac{\partial Q}{\partial t}+\frac{\partial}{\partial x}\left((1+\delta)\frac{Q^2}{A}\right)+\frac{A}{\rho}\frac{\partial p}{\partial x}=N\frac{Q}{A}, \tag{5}$$

where $A(x,t)$ is the vessel cross-sectional area and $Q(x,t)$ is the flow rate. This formulation requires a constitutive model that relates pressure, $p(x,t)$ and wall deformation. $N$ represents the viscous losses, which can be derived from the expression for the velocity profile (i.e. axisymmetric, parabolic profile ($n = 2$)).

$$N=-2(n+2)\pi v,\quad \delta=\frac{1}{1+n}. \tag{6}$$

The constitutive model based on Laplace's Law that relates the pressure and area changes was defined as:

$$p=p_{\mathrm{o}}+C_{\mathrm{r}}\frac{4}{3}\frac{Eh}{A_{\mathrm{o}}}\left(\sqrt{A}-\sqrt{A_{\mathrm{o}}}\right), \tag{7}$$

where $E$ is the Elastic modulus, $h$ is the arterial wall thickness, and $A_{\mathrm{o}}$ is the cross-sectional area at pressure $p_{\mathrm{o}}$.[13,30] We considered diastole as the reference state for $A_{\mathrm{o}}$ and $p_{\mathrm{o}}$. For our validations, we considered a rigid wall in the 3D model. We applied a constant multiplier, $C_{\mathrm{r}}$, in equation 6 to enforce negligible wall deformation (changes in cross sectional area) and to obtain a rigid wall approximation in the 1D model. For this study, we set $E = 1.15$ MPa and $C_{\mathrm{r}} = 1.64$. To determine $C_{\mathrm{r}}$, we performed a set of numerical experiments by varying $C_{\mathrm{r}}$, and quantified cross-sectional area changes respect to the reference coronary cross-sectional area.

The dramatic change in diameter at the stenosis can induce vortices and flow separation. Therefore, the radial components of the velocity are no longer negligible and the 1D flow assumption results in an underestimation of the viscous and turbulent losses. In order to accurately represent the pressure drop through the stenosis, we require an additional model that accounts for the viscous and turbulent losses. In this case, we used an algebraic model proposed by Seeley and Young,[26] based on empirical data, which given the geometric definition of the lesion and the inflow conditions estimates the trans-stenotic pressure drop as

$$\Delta p=\rho\frac{Q^2}{A_{\mathrm{o}}^2}\frac{K_{\mathrm{v}}}{\mathrm{Re}}+\rho\frac{Q^2K_{\mathrm{t}}}{2A_{\mathrm{o}}^2}\left[\frac{A_{\mathrm{o}}}{A_{\mathrm{s}}}-1\right]^2, \tag{8}$$

where $Q$ is the flow rate, Re is the Reynolds number, $A_{\mathrm{o}}$ is the cross sectional area proximal to the stenosis, $A_{\mathrm{s}}$ is the minimum cross-sectional area at the stenosis, and $K_{\mathrm{v}}$ and $K_{\mathrm{t}}$ are constants defined as

$$K_{\mathrm{v}}=32\frac{L_{\mathrm{s}}}{D_{\mathrm{o}}}\frac{A_{\mathrm{o}}^2}{A_{\mathrm{s}}^2},\quad K_{\mathrm{t}}=1.52, \tag{9}$$

*where* $L_{\mathrm{s}}$ is the length of the stenosis and $D_{\mathrm{o}}$ is the proximal diameter of the vessel.

The 1D pulsatile blood flow equations were solved using the finite element method based on the formulation presented in Wan *et al.*[36] and using sparse linear solvers available in Trilinos.[32] Time step is set to $10^{-3}$ s. Validation of the 1D solver against previously published data[6] is provided in the Electronic Supplementary Material (ESM) Section 2.

### *Hybrid 1D–3D Model*

Our 1D fluid solver can be used either independently or coupled to a 3D solver. In this work, we interfaced our 1D solver with the *SimVascular* 3D finite element solver. A 1D model of the global coronary tree was obtained by extracting the vessel centerlines and a 3D model of the region of interest (stenosis) was obtained *via* direct image segmentation in *SimVascular*. The extent to of the local 3D model was defined from the proximal section of the stenosis to a distal point at least ten diameters downstream.[44] The 1D and 3D

models were coupled numerically (using semi-implicit coupling) by imposing continuity of mass and total stress at the coupling interface[2]:

$$-\sigma(\boldsymbol{u}_{3D}, p_{3D}) \cdot \boldsymbol{n} = p_{1D} \cdot \boldsymbol{n} \text{ on } \Gamma_b \tag{10}$$

$$\int_{\Gamma_b} \boldsymbol{u}_{3D} \cdot \mathbf{n} d\Gamma = q_{1D}, \tag{11}$$

where $\boldsymbol{u}_{3D}, p_{3D}$ and $u_{1D}, p_{1D}$ refer to the velocity and pressure in the 3D and 1D model respectively, $\boldsymbol{\sigma}(\boldsymbol{u}_{3D}, p_{3D})$ is the total stress tensor defined as

$$\boldsymbol{\sigma}(\boldsymbol{u}_{3D}, p_{3D}) = -p_{3D}\boldsymbol{I} + \bar{\bar{\tau}}, \tag{12}$$

$q_{1D}$ is the flow in the 1D model, $\Gamma_b$ denotes the coupling surface, and $\boldsymbol{n}$ is the coupling surface normal. The coupling is enforced by applying a Newmann type boundary condition on the 3D model boundaries, which is computed based on the 1D model solution. We use a similar approach to that described in Esmaily Moghadam *et al.*[8] First the flow rate is passed from the 3D to the 1D model, then pressure is passed from the 1D to the 3D domain *via* Eq. (10). Pressure and flow rate are exchanged between the 3D and 1D domain at each non-linear iteration.

The parameters to generate the mesh for the local 3D model of the region of interest were defined similarly to the full 3D. The mesh also included a boundary layer and local mesh refinement at the stenosis as defined in "Three-Dimensional Computational Fluid Dynamics (3D CFD)" section.

### *Zero Dimensional (0D) Boundary Conditions*

We applied a closed-loop Lumped Parameter Network (LPN) to model the heart and the distal vasculature (Fig. 2). This LPN model included specialized boundary conditions for the coronary arteries, which allowed us to replicate the effect of myocardial contraction on coronary flow.[16] The LPN model parameters can be estimated based on patient clinical data, such as cardiac output or aortic pressure. In this case, LPN parameters were defined based on healthy population average values for cardiac output and aortic pressure and the coronary artery outlet cross-sectional area from the baseline coronary tree. The same LPN model was used for the 1D, the 3D, and the hybrid 1D–3D simulations. In each case, the LPN was coupled numerically with the fluid solver. We performed simulations under hyperemic conditions to allow the estimation of FFR, the gold standard for obstructive coronary artery disease assessment. To simulate hyperemic conditions coronary artery boundary conditions were modified to reduce microvascular flow resistance by 25% compared to resting conditions. This change between rest and hyperemic conditions is expected for a healthy vascular bed.[38] No-slip boundary conditions were applied at the wall for the 3D simulations.

### *Post Processing for 3D and 1D–3D Hybrid Simulations*

We computed wall shear stress and shear rate distributions based on the velocity fields computed in the 3D model and hybrid 1D–3D model. We obtained time-averaged wall shear stress (TAWSS), time-averaged shear rate (TASR), shear rate gradient (TASRg), and maximum WSS at the location of the stenosis. The location of the stenosis is defined as the section of the coronary artery with minimum diameter. Additionally, we computed FFR based on simulated pressure data. FFR is defined as the ratio between pressure distal to the stenosis and proximal pressure (measured at the aortic root).

## RESULTS

### *Global Hemodynamics and Flow Distribution: Healthy vs. Diseased Conditions*

The global hemodynamics for a healthy and a diseased coronary tree using a 3D model, a 1D model, and a hybrid 1D–3D model are summarized in Table 1. As a result of the imposed 90% stenosis in the LAD we observed a flow reduction in this branch, which was comparable among the three different models. Systemic flows and pressures were consistent across the three models, with variations below 1 and 3%, respectively. Furthermore, right/left coronary flow distribution was maintained with maximum left flow variations of 3.26%. We also computed FFR based on the simulated pressure data and observed differences below 3% across the models. As expected for severe stenosis, FFR was indicative of potential ischemia. The threshold to consider a diagnostic of ischemia is FFR $< 0.8$.[33]

### *Comparison of 3D and 1D Models of Coronary Flow*

Flow waveforms at each of the coronary outlets, obtained from the 1D and the 3D simulations in the healthy and diseased cases, are presented in Fig. 3. We compared the flow and pressure waveforms over a cardiac cycle at each coronary outlet and we computed the root mean square error (RMSE) and cross correlation coefficient (R) between the reduced order

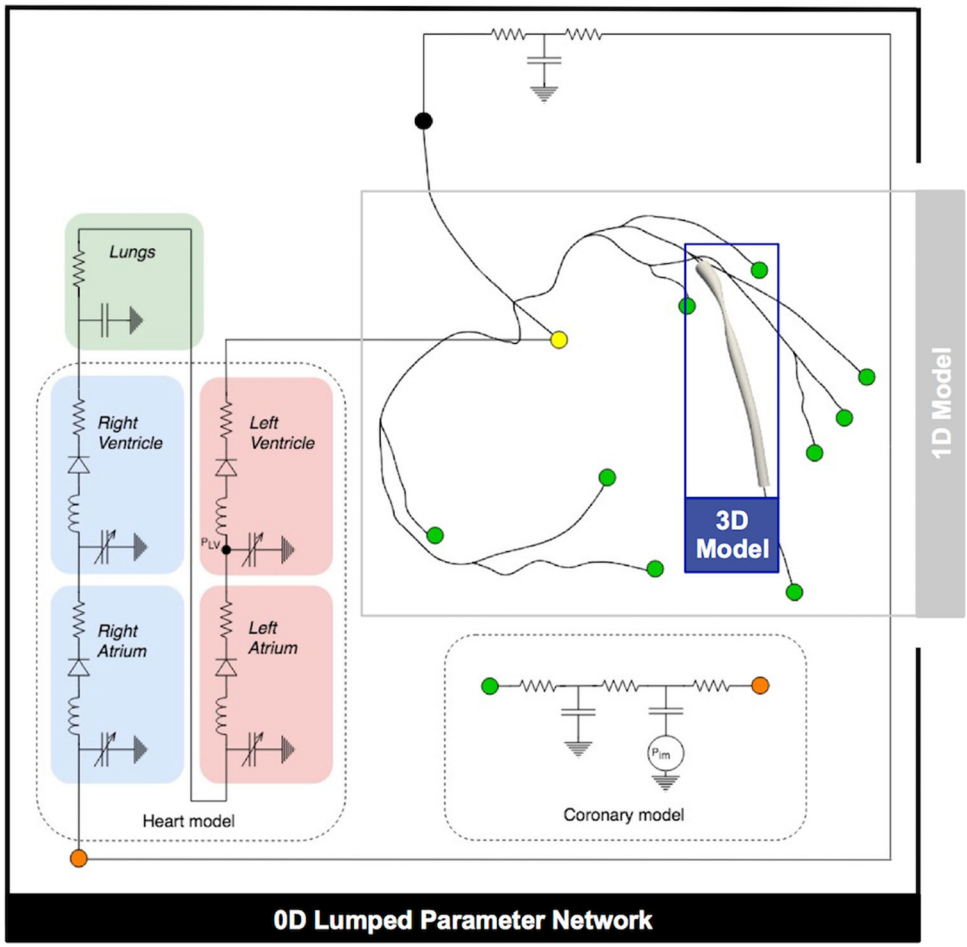


**FIGURE 2. Schematic of the 0D–1D–3D framework. A closed loop lumped parameter network is used to prescribe realistic boundary conditions including a heart model and a pulmonary circulation model, a model for the coronary micro-circulation and a three-element Windkessel model (RCR) to represent the systemic circulation. The coronary model is attached to each coronary outlet (green dot). Coronary venous return (orange dot) at each outlet is connected to the right atria (heart model) as well as the venous return from the systemic circulation. Output from the left ventricle is applied as inlet boundary condition for the 1D model (yellow dot).**

**TABLE 1. Summary of global hemodynamics**

| | Stroke volume (mL) | Left coronary volume (mL) | Right coronary volume (mL) | LAD FFR |
|---|---|---|---|---|
| 3D model (healthy) | 70.22 | 5.38 | 3.29 | 0.92 |
| 1D model (healthy) | 70.15 | 5.32 | 3.32 | 0.94 |
| 1D–3D model (healthy) | 70.00 | 5.25 | 3.30 | 0.91 |
| 3D model (LAD 90% stenosis) | 70.11 | 5.06 | 3.32 | 0.76 |
| 1D model (LAD 90% stenosis) | 70.01 | 4.89 | 3.32 | 0.76 |
| 1D–3D model (LAD 90% stenosis) | 69.9 | 4.95 | 3.31 | 0.78 |

*LAD* left anterior descending.

models flow and pressure waveforms and the reference waveforms from the full 3D simulations (Table 2). Overall differences in total outlet flow were $< 5\%$. These results confirm earlier studies[1,7,21,43] that 1D models can capture the essential features of pulsatile coronary flow for healthy and diseased vascular trees.

### *Comparison of 3D and Hybrid 1D–3D Models for Coronary Flow*

A comparison of the flow and pressure waveforms at the LAD outlet in the healthy and diseased cases using the 1D–3D hybrid model is presented in Fig. 4. Quantitative comparison of flow and pressure waveforms also is presented in Table 2. Overall differences

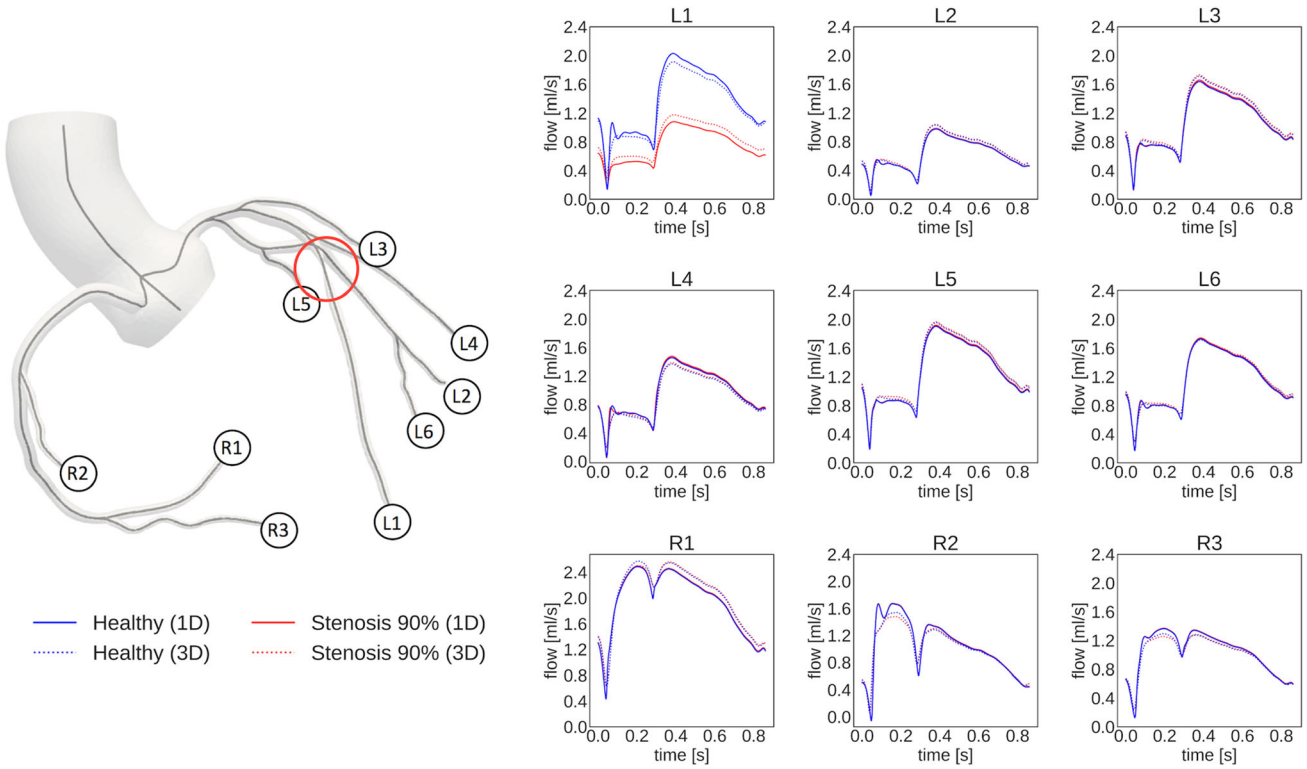


**FIGURE 3. Comparison of outlet 3D and 1D flow waveforms for healthy and diseased conditions. Left panel: reference coronary model used for simulations with a total of 9 coronary outlets (6 left outlets, 3 right outlets). Red circle indicates the location of the 90% stenosis in the disease model. Right panel: outflow waveform at each of the 9 coronary outlets. In the diseased condition, the 90% stenosis in the LAD results in 35.3% (3D) and 44.8% (1D) reduction in L1 total flow.**

in total outlet flow between 3D and 1D–3D hybrid simulations were 5%. The effect of the stenosis in terms of flow reduction and trans-stenotic pressure drop can be similarly quantified using a full 3D model and the 1D–3D hybrid model (Table 1). Flow reduction as a result of the stenosis in the LAD was 35.3% compared to the healthy case based on the 3D simulation results. The effect of the stenosis quantified based on the hybrid 1D–3D simulation results in the LAD was a 32.3% flow reduction. The impact of the stenosis on the total left coronary branch flow accounts for a 6% reduction in both cases. Animal studies have reported an effect of coronary flow on ischemic markers from a 20% coronary flow reduction (LAD).[37]

Pressure and velocity distributions between the 3D model and the hybrid model also showed good agreement (Fig. 5). Wall shear stress distributions were qualitatively similar in the models (Fig. 6). Time averaged maximum WSS at the minimum area section of the stenosis in both cases was over 100 Pa. The peak shear rate at the stenosis was 9% higher in the full 3D simulation. These extreme flows exceed the criteria for von Willebrand Factor unfolding and shear-induced platelet aggregation (SIPA).[11,22]

### *Effect of 3D Model Geometry on Local Hemodynamics*

Three different LAD stenosis models with 90% area reduction and including stenosis impacting a longer segment of the LAD (twice the length of the reference stenosis case) and an asymmetric 90% stenosis are compared in Fig. 7. We introduced asymmetry in such a way that represented plaque build-up localized on the inner curvature, as it is mostly the case.[17] We investigated the changes on local wall shear stress and shear rates as a result of asymmetry or variations in length of the focal lesion under the same global hemodynamics conditions. Results show good agreement between the 3D and the 1D–3D WSS distribution. Peak shear rates at the stenosis yielded similar errors to the baseline stenosis case (~ 10%) between the 3D and the 1D–3D model. Flow and pressure waveforms comparison including the long stenosis and an asymmetric stenosis lesion can be found in ESM Section 5. We observed distinct TAWSS spatial distribution as a result of asymmetry (Fig. 7), including extent of elevated WSS ($>10$ Pa) regions. However, flow and pressure waveforms at the LAD outlet remained similar despite changes in geometry (symmetry). Increasing the length of the stenosis reduced LAD flow and increased the trans-stenotic pressure drop ($FFR_{s90} = 0.78$ vs

**TABLE 2. Flow and pressure waveforms over a cardiac cycle at each coronary outlet**

| | L1 | L2 | L3 | L4 | L5 | L6 | R1 | R2 | R3 |
|---|---|---|---|---|---|---|---|---|---|
| 1D model (healthy) | | | | | | | | | |
| Flow (mL $s^{-1}$) | | | | | | | | | |
| RMSE | 0.085 | 0.039 | 0.054 | 0.061 | 0.048 | 0.028 | 0.110 | 0.103 | 0.051 |
| *R* | 0.993 | 0.997 | 0.999 | 0.995 | 0.999 | 0.998 | 0.990 | 0.975 | 0.995 |
| Pressure (mmHg) | | | | | | | | | |
| RMSE | 6.631 | 2.052 | 2.239 | 6.848 | 2.747 | 3.909 | 9.405 | 3.299 | 7.874 |
| *R* | 0.993 | 0.999 | 0.999 | 0.993 | 0.999 | 0.997 | 0.988 | 0.996 | 0.990 |
| 1D–3D model (healthy) | | | | | | | | | |
| Flow (mL $s^{-1}$) | | | | | | | | | |
| RMSE | 0.110 | 0.047 | 0.048 | 0.077 | 0.044 | 0.048 | 0.106 | 0.166 | 0.064 |
| *R* | 0.995 | 0.986 | 0.998 | 0.989 | 0.998 | 0.993 | 0.991 | 0.923 | 0.989 |
| Pressure (mmHg) | | | | | | | | | |
| RMSE | 1.112 | 2.138 | 2.302 | 7.038 | 2.841 | 4.053 | 9.291 | 3.915 | 7.916 |
| *R* | 0.999 | 0.998 | 0.999 | 0.992 | 0.998 | 0.996 | 0.987 | 0.988 | 0.986 |
| 1D model (LAD 90% stenosis) | | | | | | | | | |
| Flow (mL $s^{-1}$) | | | | | | | | | |
| RMSE | 0.087 | 0.040 | 0.055 | 0.062 | 0.051 | 0.031 | 0.108 | 0.114 | 0.058 |
| *R* | 0.999 | 0.997 | 0.999 | 0.994 | 0.999 | 0.998 | 0.988 | 0.971 | 0.993 |
| Pressure (mmHg) | | | | | | | | | |
| RMSE | 1.027 | 1.828 | 2.245 | 6.890 | 2.694 | 3.689 | 9.719 | 3.861 | 8.280 |
| *R* | 1.000 | 0.999 | 0.999 | 0.993 | 0.999 | 0.997 | 0.989 | 0.996 | 0.990 |
| 1D–3D model (LAD 90% stenosis) | | | | | | | | | |
| Flow (mL $s^{-1}$) | | | | | | | | | |
| RMSE | 0.054 | 0.049 | 0.053 | 0.077 | 0.050 | 0.049 | 0.104 | 0.172 | 0.068 |
| *R* | 0.989 | 0.987 | 0.998 | 0.988 | 0.998 | 0.993 | 0.990 | 0.919 | 0.988 |
| Pressure (mmHg) | | | | | | | | | |
| RMSE | 1.759 | 1.853 | 2.159 | 6.885 | 2.692 | 3.715 | 9.482 | 4.287 | 8.196 |
| *R* | 0.998 | 0.998 | 0.999 | 0.991 | 0.998 | 0.996 | 0.987 | 0.987 | 0.985 |

Reduced order model errors compared to full 3D simulation.
*LAD* left anterior descending, *RMSE* root mean squared error, *R* cross -correlation coefficient.

$FFR_{s90Long}$ = 0.61), and increased wall shear stress levels ($maxWSS_{s90}$ = 159 = Pa vs $maxWSS_{s90Long}$ = 212 Pa).

### *Analysis of Computational Cost: 3D vs. 1D–3D Hybrid Model*

The cost of the simulation in CPU hours and the dimension of the finite element mesh in each case are presented in Table 3. Using the hybrid 1D–3D model reduced the computation time by approximately a factor of 40 compared to the full 3D simulation. Such savings would be significant in situations where geometry changes (growing thrombosis) and/or global hemodynamics evolve (ischemia and infarction).

## DISCUSSION

In this computational study, we demonstrate that a hybrid 1D–3D model of the coronary arteries can estimate local hemodynamics similarly to a full 3D coronary simulation, including the spatial distribution of WSS and shear rate gradients. The characterization of WSS and shear rate gradients at the stenosis is required to model the formation of an arterial clot after plaque rupture or erosion in the setting of coronary disease. This 1D–3D coupled modeling approach reduces significantly the computational cost compared to a full 3D model of the coronary tree and therefore is suitable to be used in combination with a thrombosis model that simulates the microscopic events of thrombus formation, such as platelet deposition and aggregation, towards a fully multiscale model.

The 1D model assumes unidirectionality of the flow, however, this does not hold in the presence of a stenosis. The drastic diameter reduction could induce vortices and secondary flows downstream and therefore velocity components in other directions are no longer negligible. This typically results in an underestimation of the pressure drop through the stenosis. An algebraic pressure-drop model can be incorporated into the 1D flow model to account for viscous and turbulent losses. Our computational

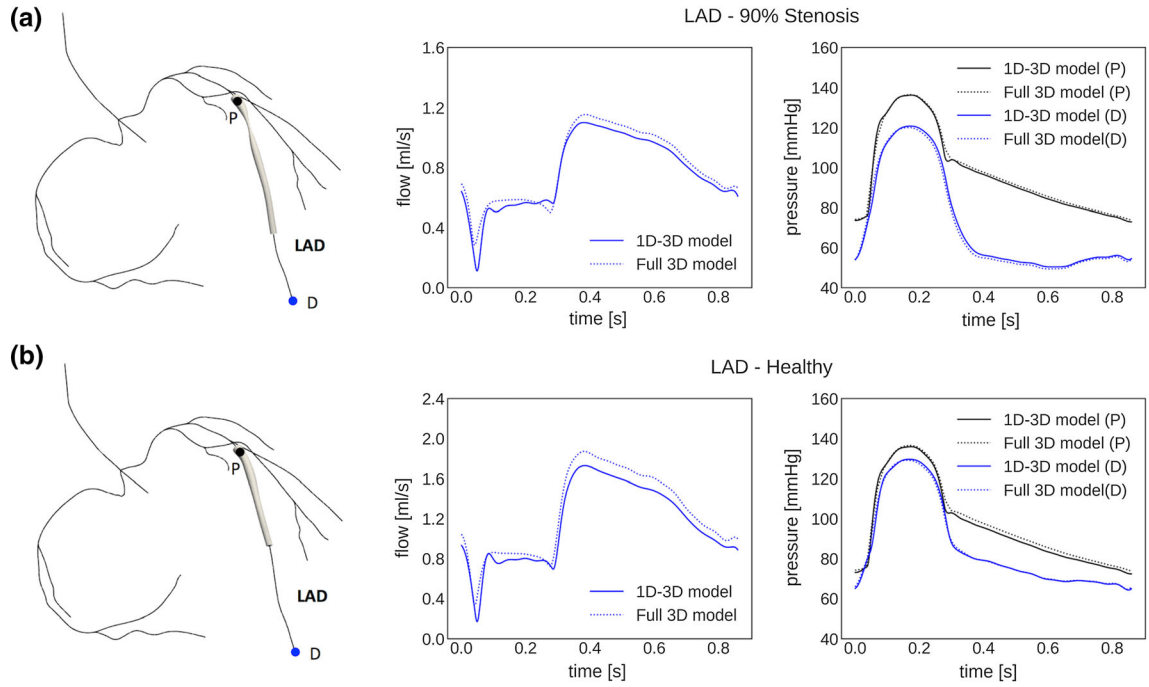


**FIGURE 4. Comparison of full 3D and hybrid 1D–3D simulation flow and pressure waveforms. (a) Hybrid 1D–3D coronary model with 90% stenosis in the LAD (diseased condition). Flow and pressure waveforms at the LAD outlet. Fractional flow reserve (FFR) for the 3D and 1D–3D models is $FFR_{3D}$=0.76 FFR1D–3D = 0.78. (b) Hybrid 1D–3D coronary model (healthy). Flow and pressure waveforms at the LAD outlet. LAD = left anterior descending, P = proximal, D = distal.**

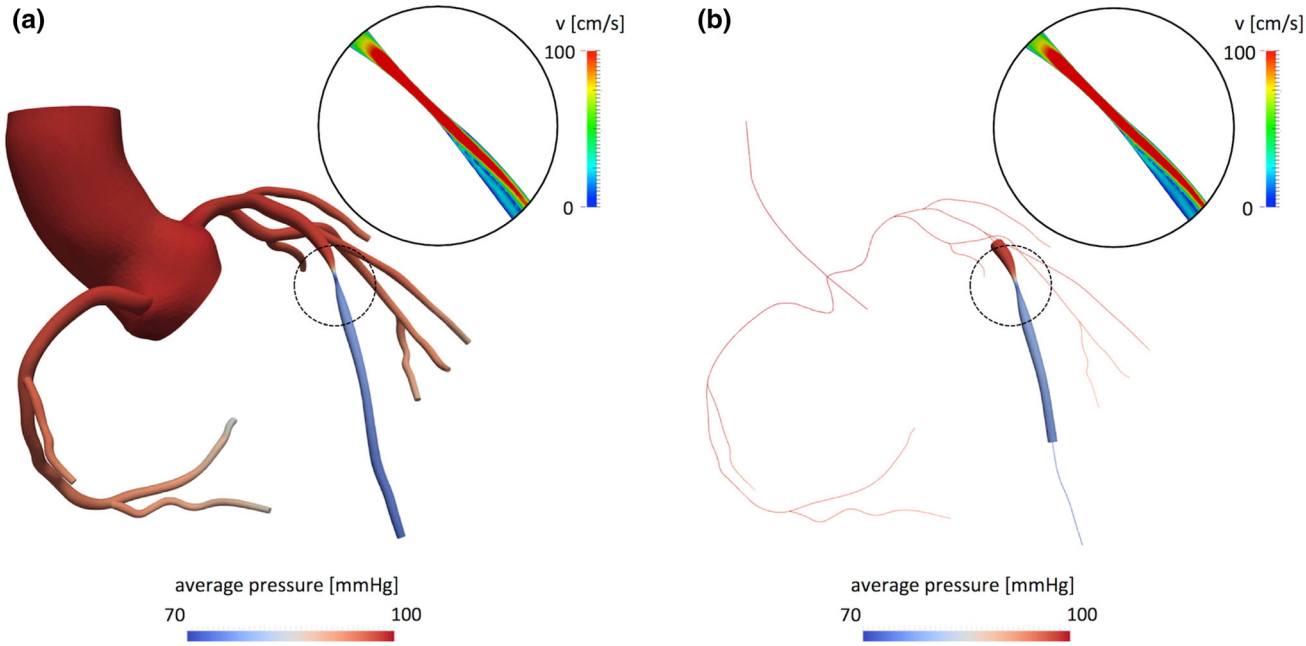


**FIGURE 5. Pressure distribution and velocity field (longitudinal slice at the location of the stenosis). (a) full 3D simulation; (b) hybrid 1D–3D simulation.**

experiments show that 1D models can be used to determine changes in global hemodynamics as a result of narrowing or stenosis with a reasonable error. However, 1D flow simulations do not provide local hemodynamic data to inform a thrombosis model. In addition, the estimation of trans-stenotic pressure drop, in this case, relies on a simplified geometric characterization of the focal lesion—length and minimum cross-sectional area—which may not fully represent the complexity of atherosclerotic lesions. On the

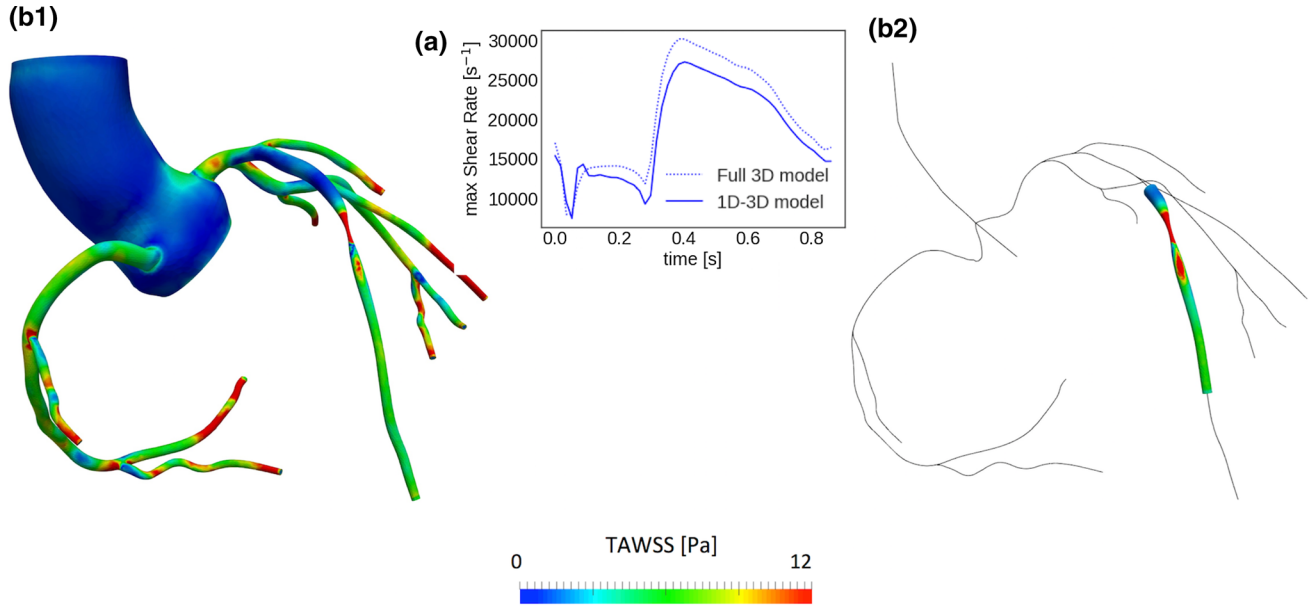


**FIGURE 6. Comparison of shear rate and wall shear stress calculation from full 3D and hybrid 1D–3D simulation results. (a) Evolution of maximum shear rate at minimum cross sectional area location over one cardiac cycle. (b) Time averaged wall shear stress distribution over one cardiac cycle. (b.1) full 3D simulation (b.2) hybrid 1D–3D simulation**

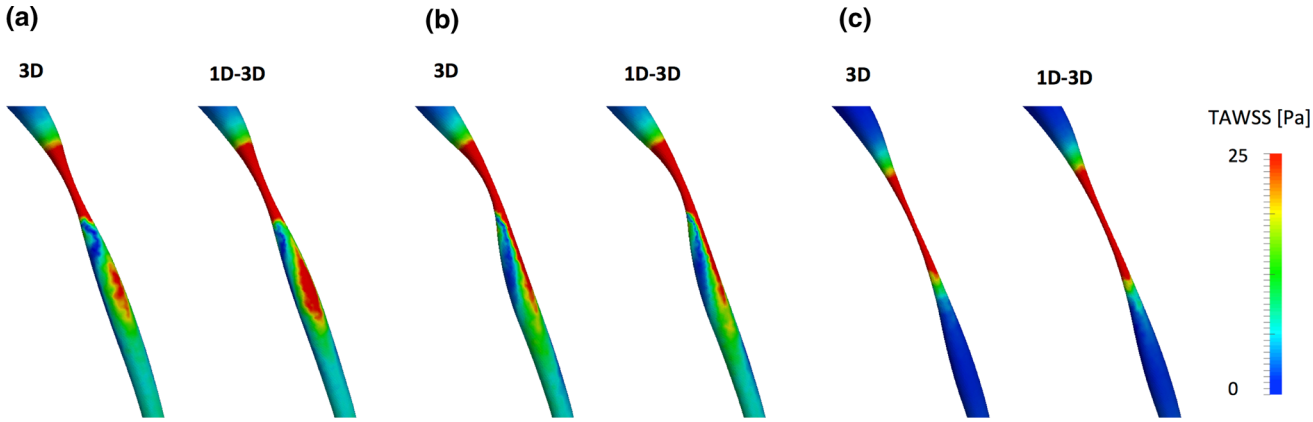


**FIGURE 7. Effect of 3D model geometry on peak (systole) wall shear stress distribution (TAWSS). (a) 90% stenosis (symmetric); (b) 90% stenosis (asymmetric); (c) 90% stenosis (symmetric, long).**

**TABLE 3. Computational cost assessment**

| | Number of mesh elements [1D/3D] | Core-hours[a] (h) |
|---|---|---|
| 3D model (healthy) | –/525,481 | 1516.67 |
| 1D model (healthy) | 644/– | 0.93 |
| 1D–3D model (healthy) | 558/37,502 | 33.2 |
| 3D model (LAD 90% stenosis) | –/657,619 | 4314.24 |
| 1D model (LAD 90% stenosis) | 634/– | 0.91 |
| 1D–3D model (LAD 90% stenosis) | 558/183,853 | 107.2 |

[a]Core-hours = total hours × number of cores.

other hand, our proposed 1D–3D framework was able to replicate the pressure and velocity fields obtained in a full 3D simulation. Besides, this approach allows incorporating a 3D description of the stenosis including shear rate gradients.

We performed a sensitivity analysis with respect to the extension of the 3D model. This analysis showed that including a longer portion of the 3D model of the region of interest (i.e. stenosis) did not change substantially the results of the simulation. We did not observe significant improvement or worsening of the WSS estimation as a result of modifying the extent of the 3D sub-model. Also, including a shorter region of interest or longer region of interest effect on the computation time was negligible respect to the full 3D computation time (ESM Section 4).

The validation of the 1D model and the hybrid 1D–3D model against a 3D model in simple geometries (i.e., the main carotid artery) showed exact overlap between the two solutions (ESM Section 3). This suggests that the differences observed in the 1D–3D coronary model solutions compared to the full 3D arise from the complexity of the anatomy. In particular, these differences may result from the curvature of the coronary arteries and the branching, which are not considered in the 1D representation. Notably, these differences are still below the typical measurement error for flow and pressure waveforms obtained invasively by catheterization.[27] Future studies should include the effect of the curvature of the vessel curvature, in particular, upstream to the 3D model.

We used the 1D–3D model to perform simulations in different LAD stenosis geometries. We observed that even for lesions similarly classified according to minimum diameter, the local WSS and WSSg fields could be substantially different. This demonstrates the need for a patient-specific approach for modeling thrombosis under flow, where shear stress gradients play a significant role in platelet aggregation. We observed differences in the velocity profile proximal to the lesion comparing the 3D and the 1D–3D models. We believe these discrepancies may be the source of the WSS and shear rate errors. Future work should consider a correction of the inlet velocity profile based on the vessel curvature or proximity to a bifurcation.

This framework also offers the possibility to solve reaction-advection-diffusion equations simultaneously with the flow, using the *SimVascular* finite element solver. Future work will be focused on this direction, including patient-specific information regarding blood biochemistry to analyze the effect of platelet-count and other blood patient-specific biochemistry in the formation of the clot.

This work introduces a significant advancement as opposed to a simple prescribed inlet flow obtained from a one-time 3D simulation. In this case, the flow conditions can be updated as the geometry changes. This dynamic coupling is essential to provide the capability of simulating the formation of a clot and the changes in flow derived from time-dependent occlusions. Moreover, we use closed-loop boundary conditions, including a heart model, which allows us to incorporate the effect of the stenosis in the ventricular function resulting from myocardial under-perfusion, as changes in the ventricular PV loop.

Here we presented several cases where the stenosis is isolated in a segment of the LAD, even including a bifurcation as the 3D region of interest. The framework is flexible and allows any section of the coronary tree to be replaced with a 3D representation. Follow up studies including patient specific coronary anatomies will focus on demonstrating that this modeling approach is prepared to deal with the complexities that may arise in a patient-specific model where atherosclerotic arteries can present diffuse lesions and/or lesions near bifurcations, as long as image segmentation is possible.

In conclusion, we have developed and validated a new framework that allows obtaining local hemodynamic data of an anatomic region of interest, coronary stenosis, with similar accuracy to a full 3D simulation of the coronary tree, but with a significantly reduced computational cost. Future work will focus on incorporating reaction-advection-diffusion equations into the model to simulate the evolution of chemical agonists near the stenotic lesion and track their accumulation in post stenosis recirculation areas. We expect that this modeling framework provides not only a tool to investigate adverse cardiovascular outcomes such as coronary thrombosis, but also a test-bed for anticoagulation drug testing.

## SUPPLEMENTARY INFORMATION

The online version contains supplementary material available at https://doi.org/10.1007/s13239-021-00580-5.

## FUNDING

This work was supported by R01-HL-103419 (N.G.G and S.L.D).

## DATA AVAILABILITY

Not applicable.

## CODE AVAILABILITY

Code developed for this study will be available *via* online code repository.

## CONFLICT OF INTEREST

The authors declare that they have no conflict of interest.

## REFERENCES


[1]Blanco, P. J., C. A. Bulant, L. O. Müller, G. D. M. Talou, C. G. Bezerra, P. A. Lemos, and R. A. Feijóo. Comparison of 1D and 3D models for the estimation of fractional flow reserve. *Sci. Rep.* 8:1–12, 2018.

[2]Blanco, P. J., and R. A. Feijóo. A dimensionally-heterogeneous closed-loop model for the cardiovascular system and its applications. *Med. Eng. Phys.* 35:652–667, 2013.

[3]Blanco, P. J., M. R. Pivello, S. A. Urquiza, and R. A. Feijóo. On the potentialities of 3D–1D coupled models in hemodynamics simulations. *J. Biomech.* 42:919–930, 2009.

[4]Blanco, P. J., S. A. Urquiza, and R. A. Feijóo. Assessing the influence of heart rate in local hemodynamics through coupled 3D–1D–0D models. *Int. J. Numer. Method. Biomed. Eng.* 26:890–903, 2010.

[5]Bluestein, D., L. Niu, R. T. Schoephoerster, and M. K. Dewanjee. Fluid mechanics of arterial stenosis: relationship to the development of mural thrombus. *Ann. Biomed. Eng.* 25:344–356, 1997.

[6]Boileau, E., P. Nithiarasu, P. J. Blanco, L. O. Müller, F. E. Fossan, L. R. Hellevik, W. P. Donders, W. Huberts, M. Willemet, and J. Alastruey. A benchmark study of numerical schemes for one-dimensional arterial blood flow modelling. *Int. J. Numer. Method Biomed. Eng.* 31:1–33, 2015.

[7]Boileau, E., S. Pant, C. Roobottom, I. Sazonov, J. Deng, X. Xie, and P. Nithiarasu. Estimating the accuracy of a reduced-order model for the calculation of fractional flow reserve (FFR). *Int. J. Numer. Method Biomed. Eng.* 2018. https://doi.org/10.1002/cnm.2908.

[8]Esmaily Moghadam, M., I. E. Vignon-Clementel, R. Figliola, and A. L. Marsden. A modular numerical method for implicit 0D/3D coupling in cardiovascular finite element simulations. *J. Comput. Phys.* 244:63–79, 2013.

[9]Flamm, M. H., and S. L. Diamond. Multiscale systems biology and physics of thrombosis under flow. *Ann. Biomed. Eng.* 40:2355–2364, 2012.

[10]Fleeter, C. M., G. Geraci, D. E. Schiavazzi, A. M. Kahn, and A. L. Marsden. Multilevel and multifidelity uncertainty quantification for cardiovascular hemodynamics. *Comput. Methods Appl. Mech. Eng.* 2020. https://doi.org/10.1016/j.cma.2020.113030.

[11]Fogelson, A. L., and K. B. Neeves. Fluid mechanics of blood clot formation. *Annu. Rev. Fluid. Mech.* 47:377–403, 2015.

[12]Formaggia, L., J.-F. Gerbeau, F. Nobile, and A. Quarteroni. On the coupling of 3D and 1D Navier-Stokes equations for flow problems in compliant vessels. *Comput. Methods Appl. Mech. Eng.* 191:561–582, 2001.

[13]Formaggia, L., D. Lamponi, and A. Quarteroni. One-dimensional models for blood flow in arteries. *J. Eng. Math.* 47:251–276, 2003.

[14]Fossan, F. E., J. Sturdy, L. O. Müller, A. Strand, A. T. Bråten, A. Jørgensen, R. Wiseth, and L. R. Hellevik. Uncertainty quantification and sensitivity analysis for computational FFR estimation in stable coronary artery disease. *Cardiovasc. Eng. Technol.* 9:597–622, 2018.

[15]Hughes, T. J. R., and J. Lubliner. On the one-dimensional theory of blood flow in the larger vessels. *Math. Biosci.* 18:161–170, 1973.

[16]Kim, H. J., I. E. Vignon-Clementel, J. S. Coogan, C. A. Figueroa, K. E. Jansen, and C. A. Taylor. Patient-specific modeling of blood flow and pressure in human coronary arteries. *Ann. Biomed. Eng.* 38:3195–3209, 2010.

[17]Krams, R., J. J. Wentzel, J. A. F. Oomen, R. Vinke, J. C. H. Schuurbiers, P. J. de Feyter, P. W. Serruys, and C. J. Slager. Evaluation of endothelial shear stress and 3d geometry as factors determining the development of atherosclerosis and remodeling in human coronary arteries in vivo. *Arterioscler. Thromb. Vasc. Biol.* 17:2061–2065, 1997.

[18]Leiderman, K., and A. L. Fogelson. Grow with the flow: a spatial-temporal model of platelet deposition and blood coagulation under flow. *Math. Med. Biol.* 28:47–84, 2011.

[19]Lu, Y., M. Y. Lee, S. Zhu, T. Sinno, and S. L. Diamond. Multiscale simulation of thrombus growth and vessel occlusion triggered by collagen/tissue factor using a data-driven model of combinatorial platelet signalling. *Math. Med. Biol.* 34:523–546, 2017.

[20]Mahmoudi, M., A. Farghadan, D. R. McConnell, A. J. Barker, J. J. Wentzel, M. J. Budoff, and A. Arzani. The story of wall shear stress in coronary artery atherosclerosis: biochemical transport and mechanotransduction. *J. Biomech. Eng.* 2021. https://doi.org/10.1115/1.4049026.

[21]Mirramezani, M., S. Diamond, H. Litt, and S. C. Shadden. Reduced order models for transstenotic pressure drop in the coronary arteries. *J Biomech Eng*. 2018. https://doi.org/10.1115/1.4042184.

[22]Moake, J. L., N. A. Turner, N. A. Stathopoulos, L. H. Nolasco, and J. D. Hellums. Involvement of large plasma von Willebrand factor (vWF) multimers and unusually large vWF forms derived from endothelial cells in shear stress-induced platelet aggregation. *J. Clin. Invest.* 78:1456–1461, 1986.

[23]Nesbitt, W. S., E. Westein, F. J. Tovar-Lopez, E. Tolouei, A. Mitchell, J. Fu, J. Carberry, A. Fouras, and S. P. Jackson. A shear gradient-dependent platelet aggregation mechanism drives thrombus formation. *Nat. Med.* 15:665–673, 2009.

[24]Nobile, F. Coupling strategies for the numerical simulation of blood flow in deformable arteries by 3D and 1D models. *Math. Comput. Model.* 49:2152–2160, 2009.

[25]Nobili, M., J. Sheriff, U. Morbiducci, A. Redaelli, and D. Bluestein. Platelet activation due to hemodynamic shear stresses: damage accumulation model and comparison to in vitro measurements. *ASAIO J.* 54:64–72, 2008.

[26]Seeley, B. D., and D. F. Young. Effect of geometry on pressure losses across models of arterial stenoses. *J. Biomech.* 9:439–448, 1976.

[27]Seo, J., D. E. Schiavazzi, A. M. Kahn, and A. L. Marsden. The effects of clinically-derived parametric data uncertainty in patient-specific coronary simulations with deformable walls. *Int. J. Numer. Method. Biomed. Eng.* 2020. https://doi.org/10.1002/cnm.3351.

[28]Sheriff, J., D. Bluestein, G. Girdhar, and J. Jesty. High-shear stress sensitizes platelets to subsequent low-shear conditions. *Ann. Biomed. Eng.* 38:1442–1450, 2010.

[29]Sheriff, J., J. S. Soares, M. Xenos, J. Jesty, M. J. Slepian, and D. Bluestein. Evaluation of shear-induced platelet activation models under constant and dynamic shear stress loading conditions relevant to devices. *Ann. Biomed. Eng.* 41:1279–1296, 2013.

[30]Sherwin, S. J., V. Franke, J. Peiró, and K. Parker. One-dimensional modelling of a vascular network in space-time variables. *J. Eng. Math.* 47:217–250, 2003.
[31]Si, H. TetGen, a Delaunay-based quality tetrahedral mesh generator. *ACM Trans. Math. Softw.* 41:11, 2015.
[32]Team, T. T. P. The Trilinos Project Website, 2020. At https://trilinos.github.io.
[33]Tonino, P. A. L., B. De Bruyne, N. H. J. Pijls, U. Siebert, F. Ikeno, M. vant Veer, V. Klauss, G. Manoharan, T. Engstrøm, and K. G. Oldroyd. Fractional flow reserve versus angiography for guiding percutaneous coronary intervention. *N. Engl. J. Med.* 360:213–224, 2009.
[34]Updegrove, A., N. M. Wilson, J. Merkow, H. Lan, A. L. Marsden, and S. C. Shadden. SimVascular: an open source pipeline for cardiovascular simulation. *Ann. Biomed. Eng.* 45:525–541, 2017.
[35]Urquiza, S. A., P. J. Blanco, M. J. Vénere, and R. A. Feijóo. Multidimensional modelling for the carotid artery blood flow. *Comput. Methods Appl. Mech. Eng.* 195:4002–4017, 2006.
[36]Wan, J., B. Steele, S. A. Spicer, S. Strohband, G. R. Feijóo, T. J. Hughes, and C. A. Taylor. A one-dimensional finite element method for simulation-based medical planning for cardiovascular disease. *Comput. Methods Biomech. Biomed. Eng.* 5:195–206, 2002.
[37]Watanabe, I., T. A. Johnson, J. Buchanan, C. L. Engle, and L. S. Gettes. Effect of graded coronary flow reduction on ionic, electrical, and mechanical indexes of ischemia in the pig. *Circulation.* 76:1127–1134, 1987.
[38]Wilson, R. F., K. Wyche, B. V. Christensen, S. Zimmer, and D. D. Laxson. Effects of adenosine on human coronary arterial circulation. *Circulation.* 82:1595–1606, 1990.
[39]Xiao, N., J. Alastruey, and C. Alberto Figueroa. A systematic comparison between 1-D and 3-D hemodynamics in compliant arterial models. *Int. J. Numer. Method. Biomed. Eng.* 30:204–231, 2014.
[40]Xu, Z., N. Chen, M. M. Kamocka, E. D. Rosen, and M. Alber. A multiscale model of thrombus development. *J. R. Soc. Interface.* 5:705–722, 2008.
[41]Xu, Z., N. Chen, S. C. Shadden, J. E. Marsden, M. M. Kamocka, E. D. Rosen, and M. Alber. Study of blood flow impact on growth of thrombi using a multiscale model. *Soft Matter.* 5:769–779, 2009.
[42]Yazdani, A., H. Li, J. D. Humphrey, and G. E. Karniadakis. A general shear-dependent model for thrombus formation. *PLoS Comput. Biol.* 2017. https://doi.org/10.1371/journal.pcbi.1005291.
[43]Yin, M., A. Yazdani, and G. E. Karniadakis. One-dimensional modeling of fractional flow reserve in coronary artery disease: uncertainty quantification and Bayesian optimization. *Comput. Methods Appl. Mech. Eng.* 353:66–85, 2019.
[44]Young, D. F. Fluid mechanics of arterial stenoses. *J. Biomech. Eng.* 101:157–175, 1979.
[45]Zheng, X., A. Yazdani, H. Li, J. D. Humphrey, and G. E. Karniadakis. A three-dimensional phase-field model for multiscale modeling of thrombus biomechanics in blood vessels. *PLoS Comput. Biol.* 2020. https://doi.org/10.1371/journal.pcbi.1007709.